Dynamics of Microtubule Depolymerization in Monocytes

Lynne U. Cassimeris, Patricia Wadsworth, and E. D. Salmon

Department of Biology, University of North Carolina, Chapel Hill, North Carolina 27514. Dr. Wadsworth's present address is Department of Zoology, University of Massachusetts, Amherst, Massachusetts 01003.

Abstract. Human monocytes, which contain few interphase microtubules (35.4 ± 7.7), were used to study the dynamics of microtubule depolymerization. Steady-state microtubule assembly was abruptly blocked with either high concentrations of nocodazole (10 μg/ml) or exposure to cold temperature (3°C). At various times after inhibition of assembly, cells were processed for anti-tubulin immunofluorescence microscopy. Stained cells were observed with an intensified video camera attached to the fluorescence microscope. A tracing of the entire length of each individual microtubule was made from the image on the television monitor by focusing up and down through the cell. The tracings were then digitized into a computer. All microtubules were seen to originate from the centrosome, with an average length in control cells of 7.1 ± 2.7 μm (n = 957 microtubules). During depolymerization, the total microtubule polymer and the number of microtubules per cell decreased rapidly. In contrast, there was a slow decrease in the average length of the persisting microtubules. The half-time for both the loss of total microtubule polymer and microtubule number per cell was ~40 s for nocodazole-treated cells. The rate-limiting step in the depolymerization process was the rate of initiation of disassembly. Once initiated, depolymerization appeared catastrophic. Further kinetic analysis revealed two classes of microtubules: 70% of the microtubule population was very labile and initiated depolymerization at a rate ~23 times faster than a minor population of persistent microtubules. Cold treatment yielded qualitatively similar characteristics of depolymerization, but the initiation rates were slower. In both cases there was a significant asynchrony and heterogeneity in the initiation of depolymerization among the population of microtubules.

DURING interphase, animal cells contain a cytoplasmic microtubule complex (CMTC),[1] within which the majority of microtubules extend radially from the region of a juxtanuclear centrosome or microtubule organizing center (3, 30). Microtubule assembly in living cells is initiated at the microtubule organizing center (3, 7, 29), and purified centrosomes nucleate the end-wise polymerization of microtubules in vitro (27, 28). The CMTC is a dynamic and labile structure that exists in some form of reversible monomer–polymer equilibrium with a cellular pool of tubulin subunits (14).

Several models have been proposed to explain steady-state tubulin–microtubule exchange in living cells. First, microtubules may be exchanging subunits all along their length, as initially proposed by Inoue from birefringence studies of the dynamics of mitotic spindle fiber assembly (13, 14). Second, microtubules may be in a simple equilibrium with the tubulin pool, changing length slowly by association–dissociation reactions at the microtubule ends (10, 16). Third, tubulin flux through microtubules may occur by preferential assembly at one end and disassembly at the other end, as originally described by Margolis and Wilson (23, 24). The energy driving this treadmilling process was proposed to be derived from the hydrolysis of tubulin-bound GTP which occurs after tubulin incorporation into a microtubule (23, 24).

Recent in vitro studies by Mitchison and Kirschner (27, 28) suggest that microtubules can exist in two distinct, persistent phases: a "growing" phase and a rapid "shrinking" phase. The transition between these phases is postulated to be regulated by the hydrolysis of GTP. As elongation proceeds, GTP ligated to tubulin within the core of the microtubule is hydrolyzed to GDP. Tubulin–GTP subunits are proposed to act as a cap at the microtubule ends, which permits continued microtubule growth. When hydrolysis of tubulin–GTP catches up with elongation, the tubulin–GDP core is exposed and a rapid, catastrophic, and extensive depolymerization occurs.

A unique prediction of this Dynamic Instability model is the individuality of microtubule behavior. At steady-state, microtubules do not maintain a constant equilibrium length. Instead they are continually growing or shortening. Asynchronous behavior is achieved if the rate of interconversion is a random process among the population of microtubules. This behavior was observed by Mitchison and Kirschner for mi-

1. *Abbreviations used in this paper:* CMTC, cytoplasmic microtubule complex; FRAP, fluorescence redistribution after photobleaching; MAPs, microtubule associated proteins; saline G, a solution of 2 mM phosphate buffer, 0.137 mM NaCl, 5 mM KCl, 0.6 mM $MgSO_4$, 0.1 mM $CaCl_2$, pH 7.3.

crotubules assembled in vitro from purified neuronal tubulin onto isolated centrosomes. When the exogenous tubulin pool was diluted to reduce the rate of microtubule elongation, a heterogeneous response of the microtubule population was observed. Some microtubules did not shorten, while others depolymerized rapidly and completely. The rate of decrease in total polymer appeared limited by the rate of conversion of individual microtubules from a stable to a labile state (27, 28). This result was in contrast to the reported behavior of microtubules reassembled in vitro from tubulin plus microtubule associated proteins (MAPs) (16) or microtubules in lysed cell models (8, 35), where a synchronous response, with simultaneous, end-dependent depolymerization of the entire population was observed after dilution of the tubulin pool.

Direct measurements of the dynamics of microtubules in living cells are necessary to discriminate among the proposed models for microtubule assembly, since the behavior of microtubules is likely to depend on a variety of cellular factors such as MAPs, microtubule organizing centers, tubulin modifications, and physiological conditions. Previously, the overall pattern of spindle microtubule disassembly in metaphase cells has been investigated by microinjection of colchicine or colchicine ligation to tubulin into cells to abruptly block polymerization. Polarization microscopy was used to follow the loss of microtubule polymer by measurements of changes in spindle birefringent retardation (32, 42). Microtubule depolymerization was rapid (the half-time for depolymerization was 6.5 s), and the density of microtubules decreased uniformly throughout the spindle (32, 42), but individual microtubule behavior was not resolved. The incorporation of tubulin into microtubules in vivo has been followed by microinjecting fluorescent tubulin, as a tracer of the endogenous tubulin pool (20, 31, 33, 40–42), and by measurements of fluorescence redistribution after photobleaching (FRAP) (31, 33, 41, 42). Fluorescent tubulin was found to incorporate uniformly throughout the nonkinetochore spindle fibers within ~1 min (34) and throughout the CMTC within 10–15 min (20, 33). Results of the FRAP studies are inconsistent with the simple equilibrium or treadmilling models of steady-state microtubule polymerization (31, 33, 34, 41, 42). They are consistent either with the asynchronous microtubule assembly behavior predicted by the Dynamic Instability model (27, 28) or the exchange of subunits all along the length of microtubules as proposed by the Dynamic Equilibrium model (13, 14). Soltys and Borisy (38) have recently found that fluorescent tubulin incorporates only onto the distal ends of cytoplasmic microtubules, which is unexpected from the latter proposal that subunits can intercalate all along the length of microtubules.

To obtain information concerning the pattern of microtubule disassembly in vivo, we examined this process by immunofluorescent staining of cytoplasmic microtubules in interphase PtK1 and BSC1 mammalian tissue culture cells at various intervals after treatment with nocodazole (10 μg/ml) to abruptly block microtubule assembly. Nocodazole binds rapidly to the colchicine binding site on tubulin, and this complex acts by a mechanism similiar to the tubulin–colchicine complex to block microtubule elongation (12, 21). Whereas colchicine enters cells slowly and binds to tubulin slowly, nocodazole rapidly diffuses into cells and rapidly binds to tubulin (12, 32). Spindle microtubule depolymerization in PtK1 and BSC1 cells had a half-time of <10 s, which demonstrates that nocodazole at a concentration of 10 μg/ml rapidly binds to tubulin subunits in vivo (Salmon, E.D., unpublished observations). Cytoplasmic microtubule depolymerization, in BSC1 and PtK1 cells, had a half-time of ~100 s and appeared very heterogeneous. No wave of depolymerization from the cell periphery towards the centrosome was apparent; microtubule density decreased uniformly throughout the cytoplasm (6). However, because these cells contain several hundred microtubules, individual microtubules could not be tracked along their entire length during depolymerization, and the behavior of individual microtubules could not be followed accurately.

To follow the depolymerization of individual microtubules in vivo, we looked for a cell type with relatively few cytoplasmic microtubules. Information in the literature indicated that white blood cells would be appropriate for our studies. They contain ~35 cytoplasmic microtubules (1, 36) whose entire lengths can be measured when the cells are spread on coverslips. We chose to study monocytes, in part because their microtubules were distinctly labeled after our fixation method. Microtubule assembly was abruptly blocked with nocodazole (10 μg/ml) and the disassembly of individual microtubules tracked. The results using nocodazole were compared with the behavior of microtubules after treatment at 3°C to induce disassembly. In either case, the kinetics and patterns of depolymerization demonstrate the individuality and heterogeneity of microtubule behavior.

Materials and Methods

White Blood Cells

Human white cells were obtained by allowing whole blood to clot on coverslips that had been precoated with 5% human serum, at 37°C for 20 min in a humid chamber. Blood clots were removed from the coverslips by gently pulling the clot away while the coverslips were immersed in saline G (2 mM phosphate buffer, 0.137 mM NaCl, 5 mM KCl, 0.6 mM $MgSO_4$, 0.1 mM $CaCl_2$, pH 7.3). Coverslips were then rinsed in several changes of saline G to remove red blood cells. The coverslips were flooded with saline G and returned to a humid chamber at 37°C for 20–30 min to allow the remaining adherent cells time to spread.

Alternatively, a preparation of partially purified monocytes was obtained from the laboratory of Dr. M. Cohen. This preparation normally consists of 70% lymphocytes and 30% monocytes. 20–50 μl of a cell suspension, normally containing 1.5×10^6 cells/ml, was placed on a coverslip in a humid chamber at 37°C. After 20 min cells were processed as described below.

Microtubule Depolymerization and Indirect Immunofluorescence

Nocodazole (methyl-5-(2-thienylcarbonyl)-1H-benzimidazol-2-yl carbamate, Sigma Chemical Co., St. Louis, MO) was prepared as a stock solution of 10 mg/ml in dimethylsulfoxide then diluted to a final concentration of 10 μg/ml in saline G. Coverslips were treated for various times with this nocodazole solution at 37°C and were then fixed and processed for immunofluorescence by a modification of the procedure of Karsenti et al. (19). This procedure, with brief lysis of cells before fixation, gives very clear images of the microtubules with little background staining from the tubulin pool. Cells were lysed for 15 s in 80 mM Pipes, 5 mM EGTA, 1 mM $MgCl_2$ pH 6.8, 0.5% Triton X-100. Lysis in this buffer has been shown to stabilize microtubule arrays for up to 50 min, with no observable alterations in the microtubule immunofluorescent staining patterns when compared with control, unlysed cells (19, 35). After lysis the coverslips were fixed for 10 min in 2% paraformaldehyde, 0.1% glutaraldehyde in phosphate-buffered saline (PBS, 0.137 M NaCl, 2.7 mM KCl, 1.5 mM KH_2PO_4, 8 mM Na_2HPO_4), pH 7.3, washed in PBS, extracted in −20°C methanol for 6 min and −20°C acetone for 1 min, rehydrated in PBS, briefly rinsed (5 min) in PBS, 1% bovine serum albumin (BSA), 0.1% Tween-20, and finally rinsed again with PBS. Coverslips were then incubated with 50 μl of a

monoclonal antibody to β-tubulin (37) for 2 h in a humid chamber at room temperature, or 30 min at 37°C. They were next rinsed in PBS and incubated with 50 μl of a 1:25 dilution of rhodamine-conjugated goat anti-mouse IgG (Cappel Laboratories, Cochranville, PA) for 2 h at room temperature or 30 min at 37°C. A tertiary antibody of rhodamine conjugated-rabbit anti-goat IgG (1:50 dilution; Cappel Laboratories) was used to amplify the fluorescence signal. Coverslips were rinsed with PBS and mounted in Gelvatol (Monsanto Co., St. Louis, MO).

Exposure to cold temperature was also used to depolymerize cytoplasmic microtubules. Coverslips with attached monocytes were placed in saline G precooled to 3°C. Cooling of the coverslips, from 37°C to 3°C, as measured with a Tele-Thermometer (Yellow Springs Instrument Co., Yellow Springs, OH), occurred within 8 s. After various times, the cells were lysed, fixed, and processed for immunofluorescence as described above.

Microscopy and Length Determinations

For photography, cells were imaged with a Zeiss 63×/1.4 numerical aperture planapo lens on a Zeiss Universal microscope (Carl Zeiss, Inc., Thornwood, NY) equipped for epifluorescence. Cells were photographed using Tri-X pan (Kodak) and developed in Kodak HC110.

To determine the length of each microtubule, the fluorescent images of the cells were projected onto either a Venus DV2 or an MTI Sit 66 low light level camera attached to the fluorescence microscope and viewed using a Sanyo T. V. monitor (Model VM 4208). The fluorescent image of a cell was recorded, with a Sony videocassette recorder (Model VO-5800H), while focusing up and down through the cell. The contour length of each microtubule was then traced onto a 6″ × 4″ sheet of transparent acetate. Because the 63× planapo lens has a very shallow depth of field, all microtubules cannot be followed in a single photograph. By projecting the image onto a T. V. monitor, at a total magnification of ~6,000, and focusing up and down through the specimen, the contour length of a microtubule can be accurately traced onto acetate. This procedure can be repeated for all microtubules in the cell to generate a two-dimensional projection of the CMTC. Since the images were first recorded on video tape, the microtubule patterns could be followed repeatedly, without loss of information due to bleaching of fluorescence. By focusing up and down through 15 cells, average cell height was found to be ~2 μm.

Data Analysis

The microtubule tracings were digitized with a HiPad Digitizer (Houston Instrument, Austin, TX) and an Apple II Plus computer (Apple Computer Inc., Cupertino, CA). A program was designed to calculate individual microtubule lengths, the mean length (±SD), and the number of microtubules per cell. The image of the digitized cell was also drawn on the computer screen and printed, along with the above data, with an Epson model MX-80F/T printer.

27–45 cells per time point were traced onto acetate for the nocodazole experiments; the total number of microtubules measured was 3,228. For cold-induced depolymerization, 10 cells were traced at each time point, and 921 individual microtubules were measured. Statistical analysis was done with an IBM 3081 computer (IBM Instruments, Inc., Danbury, CT). Student's *t*-test was performed by standard methods (22).

There was a small error involved in tracing a three-dimensional microtubule array onto a two-dimensional sheet of acetate. The amount of error was estimated by drawing a right triangle with a base of 7.1 μm (mean microtubule length) and a height of 2 μm (estimate of cell height). The hypotenuse of this triangle was calculated to be 7.4 μm. Thus, a microtubule projecting out from the centrosome at an angle relative to the substrate, assuming the microtubule bends little, will have its length underestimated by a maximum of 5%.

To model possible microtubule depolymerization pathways, the length distribution of the control population was used as a starting point. This distribution is listed by the computer as the average number of microtubules per 1-μm length range (0.0–0.9 μm, 1.0–1.9 μm, etc.) An amount of polymer, equivalent to the amount lost experimentally, was then subtracted from the length distribution of the control population, and the resulting number of microtubules at each length range was compared with the length distribution determined experimentally.

Results

The Cytoplasmic Microtubule Complex of Monocytes

Fig. 1 shows fluorescence and phase contrast images of a human monocyte after staining for immunofluorescence with a monoclonal antibody to tubulin. All microtubules appeared

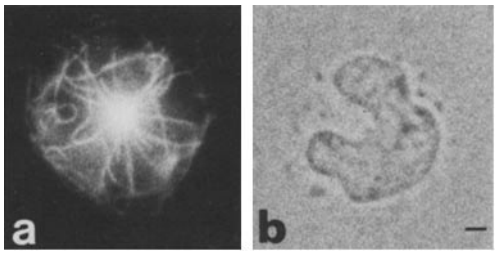

Figure 1. Immunofluorescence staining of a human monocyte with a monoclonal antibody to β-tubulin. Cells were processed for immunofluorescence as described in Materials and Methods. (*a*) Immunofluorescence and (*b*) phase-contrast images of the same cell. Microtubules radiate from the cell center to the cell periphery. The shape of the nucleus in the phase-contrast micrograph is indicative of a monocyte. Bar, 2 μm.

to radiate from the centrosome. Most microtubules were observed to end at the cell periphery, but in many cells a few microtubules extended to the cell periphery where they bent and followed the curvature of the cell perimeter for various lengths. Fig. 2, *b–d*, is a through-focal series of a monocyte photographed from the video monitor, at ~0.75-μm intervals and Fig. 2 *a* is the corresponding two-dimensional reconstruction of all microtubules within the same cell, demonstrating the accuracy of this technique. We have found these cells to contain an average of 35.4 ± 7.7 microtubules ($n = 27$). This comparatively low number of cytoplasmic microtubules allows quantitative analysis of microtubule behavior since all microtubules of each cell can be readily identified and each microtubule's length can be accurately recorded. The average length of a microtubule was 7.1 ± 2.7 μm ($n = 957$), and the average total microtubule polymer per cell was 251 ± 78 μm. Total microtubule polymer per cell was calculated by summing the lengths of all microtubules in a cell.

Depolymerization in Nocodazole

When microtubule assembly was abruptly blocked with a high concentration of nocodazole (10 μg/ml), there was a rapid decrease in both the total amount of microtubule polymer and in the mean number of microtubules per cell, but the length of remaining microtubules decreased slowly (Figs. 3, 4, 5, and 6). This striking result was clearly apparent after 30 s of incubation in nocodazole. During this time the mean number of microtubules per cell decreased by 47% (35.4–18.9; Fig. 5 *b*), while the change in mean microtubule length was insignificant (7.1–6.9 μm; Fig. 5 *c*). Statistical analysis by Student's *t*-test confirmed a significant difference in mean microtubule number ($P < 0.05$) between control cells and cells treated for 30 s with nocodazole (Fig. 5 *b*). However, the difference in mean microtubule length (Fig. 5 *c*) during this interval was not significantly different ($P > 0.05$). With longer exposure to nocodazole there was a continued loss in microtubule number, accompanied by a slow decrease in the average length of the remaining microtubules. The half-time for both the decrease in total polymer and in microtubule number was ~35–40 s (Fig. 5, *a* and *b*).

Two distinct populations of microtubules appear to exist within the cytoplasmic microtubule complex based on their differential stability to nocodazole. This is shown in the biphasic semilogarithmic plots of the kinetic data (Fig. 5, *d* and *e*). The rate constants of overall microtubule polymer loss

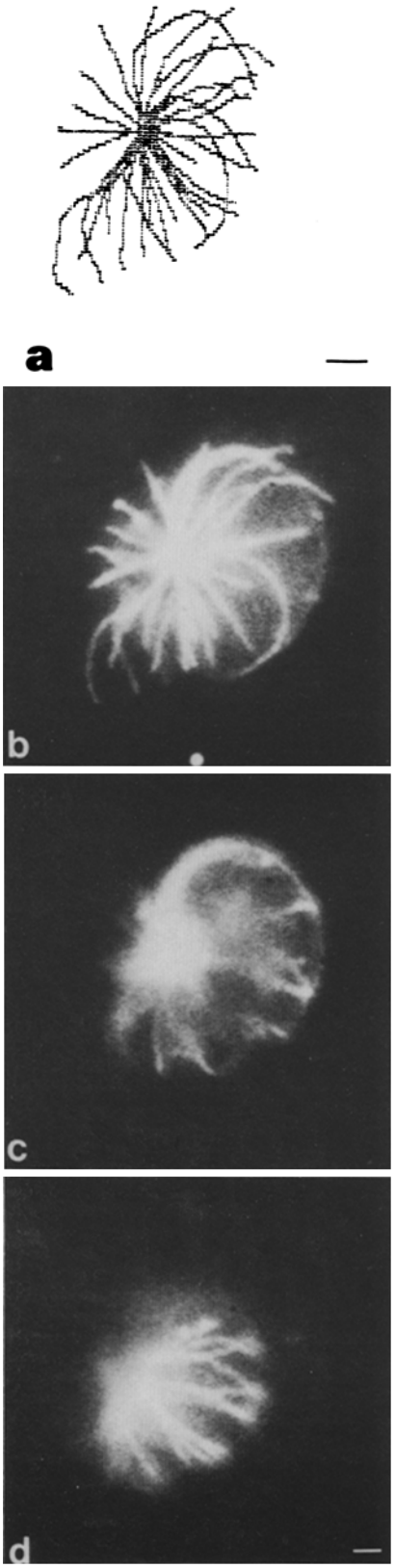

Figure 2. (*a*) The entire CMTC of a control monocyte, reconstructed as described in Materials and Methods. Bar, 2 μm. (*b, c,* and *d*) Optical sections of the same monocyte after immunofluorescent localization of tubulin. The images were photographed from the video monitor at ~0.75-μm intervals. Bar, 1 μm.

and microtubule number loss were calculated from the slopes of the semilogarithmic plots. For each case the half-time was calculated as $t_{1/2}$ = ln 2/(first order rate constant). This data is summarized in Table I. There was an ~20-fold difference in the rates of loss of polymer and microtubule numbers between the two populations. The percent of microtubules in the persistent population was determined by the intercept with the ordinate at time zero. Approximately 70% of the microtubules belonged to the labile population, while the other 30% of the microtubules were differentially stable.

The length histogram data in Fig. 6 demonstrates clearly that the rate limiting step in polymer disassembly was the rate of initiation of depolymerization and not the rate of tubulin dissociation and depolymerization of individual microtubules. The distribution of microtubule lengths changes very little during disassembly in nocodazole. The dashed lines superimposed on the histograms in Fig. 6 represent theoretical changes in microtubule length distributions if all microtubules depolymerized simultaneously at the same rate. This model was calculated from the initial distribution of microtubule lengths as described in Materials and Methods. The actual distributions of microtubule lengths were not consistent with this mechanism.

Since it appeared from Fig. 5, *d* and *e* that there were two distinct microtubule populations, a model of depolymerization of all microtubules of a particular class (labile or differentially stable) by a synchronous, end-dependent mechanism was calculated. Several assumptions were needed to calculate the theoretical length distributions. During the first minute of nocodazole exposure, the ~70% loss in total microtubule polymer was presumed to occur solely by loss of the labile population. The length distribution of the control cells was then divided into two populations; 70% of each length range was assigned to the labile population and 30% to the persistent population. Depolymerization was assumed to be independent of microtubule length, with all microtubules within a class depolymerizing synchronously at the same rate. Using these assumptions, the depolymerization was again modeled by an end-dependent, synchronous depolymerization, with the use of the labile microtubule population for the first minute and the differentially stable microtubule population for the remaining time points. This model is shown by solid lines in Fig. 6; again the experimental data are not consistent with simple, synchronous, end-wise depolymerization of the two populations.

Short microtubules, unattached to the centrosome and located near the periphery of the cell, were observed only rarely (four fragments observed in 275 cells analyzed). Fragments as small as 0.5 μm, either attached or free of the centrosome, should be visible in our preparation. To determine if small microtubule fragments were lost during the lysis step, the experiment was repeated with a 30-s incubation in nocodazole followed directly by fixation without prior detergent extraction. Although there was considerable background staining due to the cytosol tubulin pool, no fragments were observed (data not shown). Because microtubule depolymerization was rapid and complete once initiated and because so few fragments of microtubules were observed, we could not determine by our experimental protocol whether depolymerization of a single microtubule was initiated at the centrosome, at the distal end, or at sites all along the microtubule length.

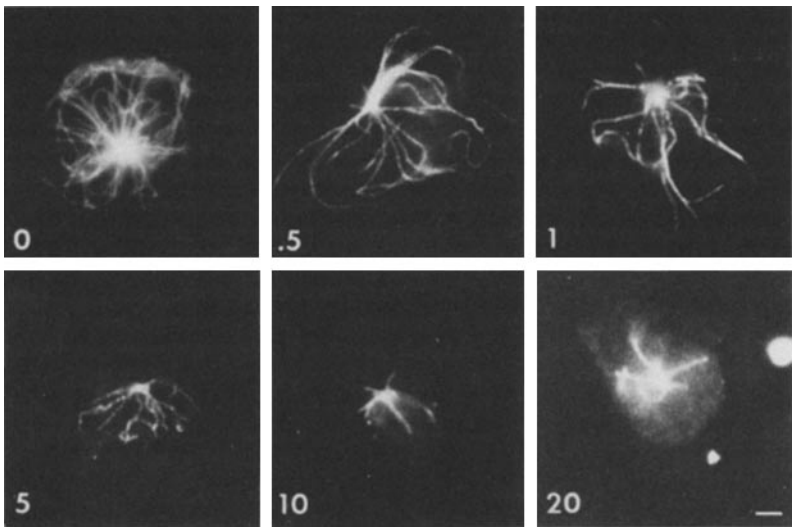

Figure 3. Tubulin immunofluorescence of cells treated with nocodazole. Cells were treated with 10 μg/ml nocodazole for the times indicated in minutes on each frame. Nearly all microtubules were seen to extend radially outward from the centrosome during all stages of the depolymerization process. Some microtubules appear segmented because of the shallow depth of field of the objective lens used. Bar, 2 μm.

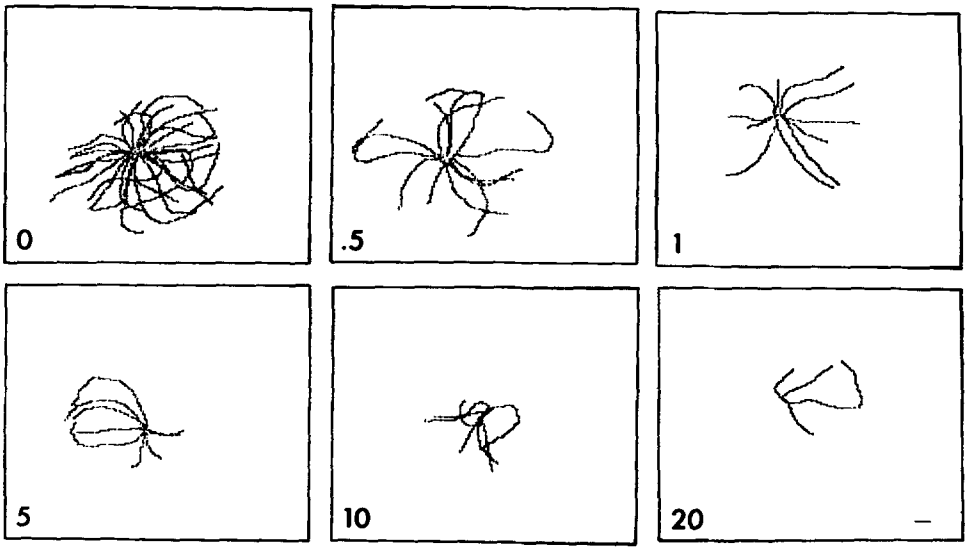

Figure 4. Examples of computer-generated line drawings of microtubule arrays obtained from single monocytes treated with nocodazole and processed for immunofluorescent staining of microtubules. The duration (in minutes) of incubation in 10 μg/ml nocodazole is indicated for each frame. These images were generated from different cells than those pictured in Fig. 3. These digitized images were used by the computer to determine the average length, the number of microtubules, and the total polymer length of the microtubules in each cell. Bar, 1 μm.

Within our 30-s sampling interval, a microtubule completely disassembles once depolymerization is initiated.

From our data we can only estimate a lower limit for the nonsteady-state rate of tubulin dissociation from the population of microtubules that rapidly initiates depolymerization. Conceptually, it is simplest to envision that in ~35 s, 50% of the microtubules have depolymerized completely, while the other 50% have remained unaffected. An apparent tubulin dissociation rate of 329 dimers/s per microtubule is required for depolymerization of a microtubule of 7.1 μm length, based on 1,625 dimers/μm, within 35 s. Since initiation of microtubule depolymerization could occur continuously over this 35-s interval, the true value of the dissociation rate constant is likely to be significantly greater than this estimate.

Depolymerization at Cold Temperature

As an alternative to nocodazole, we also blocked microtubule assembly by exposure of cells to 3°C. In general, cold treatment of cells produced a pattern of microtubule depolymerization similar to that observed with nocodazole (Figs. 7–10). As with nocodazole, there is a slow decrease in the average length of persisting microtubules, with a faster loss of microtubule number (Figs. 7–9). The half-times for number loss and total polymer loss are 2.3 min and 1.9 min, respectively (Fig. 9). Two microtubule populations are also present during cold-induced depolymerization, as shown by the semilogarithmic plots (Fig. 9, *d* and *e*), but these populations are less distinct than those observed after nocodazole treatment. The kinetic data derived from these plots are summarized in Table II. The labile population of microtubules comprises ~84% of the entire population, and the persistent population comprises the remaining 16%. With cold exposure there is a 6.4-fold difference in the rate of loss of microtubule numbers and a 1.9-fold difference in the rate of total polymer loss between the two populations.

The length distributions shown in Fig. 10 were compared with a model of synchronous microtubule disassembly by tubulin dissociation from all the microtubule ends. As shown by the dashed lines in Fig. 10, the actual microtubule length distributions during depolymerization are not consistent with this model during the early course of depolymerization. Only after drastic reduction in microtubule number and length (20 min) does the experimental data somewhat fit the theoretical model. Calculations of theoretical length distributions were also made, taking into consideration the two microtubule populations and by using assumptions similar to those made

for the nocodazole-treated cells. This model, shown by solid lines (Fig. 10), fits the data only after long exposure (20 min) to the cold temperature. As found in the nocodazole experiments, the rate of initiation of depolymerization and not the rate of microtubule shortening appears to limit the rate of depolymerization induced by cooling.

Fragments of microtubules were not observed free of the centrosome during cold-induced depolymerization. After prolonged cooling (20 min), short microtubules extending from the centrosome were seen as indicated in Fig. 10.

Microtubule depolymerization induced by cold treatment was not as rapid as that induced by nocodazole. The mean length of persisting microtubules remains at 80% of the

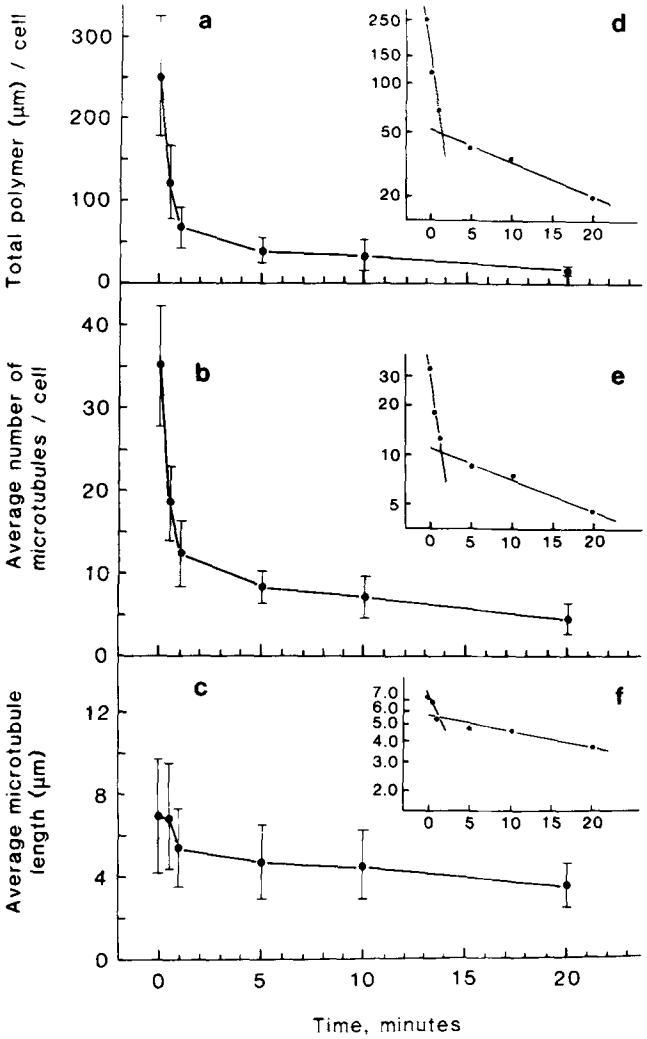

Figure 5. The changes in total polymer (*a*, linear scale; *d*, semilogarithmic scale), number of microtubules (*b*, linear scale; *e*, semilogarithmic scale) and average microtubule length (*c*, linear scale; *f*, semilogarithmic scale) per monocyte after depolymerization induced by treatment with 10 μg/ml nocodazole. Each data point represents the average of 27–45 cells, and the error bars correspond to the standard error of the mean.

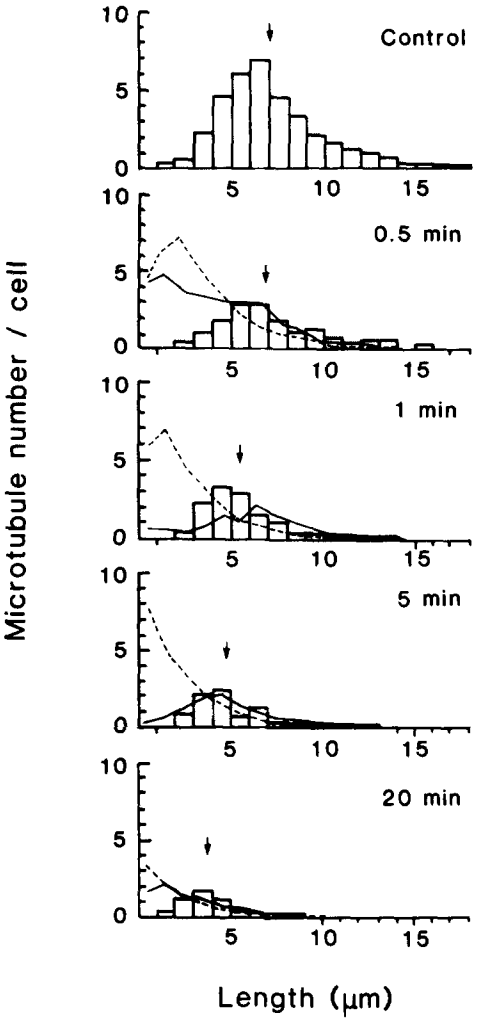

Figure 6. Histograms of the average distribution of microtubule lengths in monocytes after treatment with 10 μg/ml nocodazole for the times indicated. Each histogram represents the average microtubule length distribution derived from 27–45 cells. Arrows denote the mean length at each time point. Dashed lines represent theoretical length distributions for synchronous shortening of all microtubules at a constant rate. The extent of microtubule shortening by this mechanism was calculated to match the decrease in total polymer at each time point shown in Fig. 5*a*, as described in Materials and Methods. The solid lines show theoretical microtubule length distributions based on two microtubule populations, with different rates of polymer loss, and a synchronous disassembly within each population.

*Table I. Biphasic Kinetics of Microtubule Depolymerization in Nocodazole**

	Labile population			Differentially stable population		
	k (s^{-1})	$t_{1/2}$ (s)	%	k (s^{-1})	$t_{1/2}$ (s)	%
Loss in total polymer	1.99×10^{-2}	35	70	1.04×10^{-3}	666	30
Loss in microtubule number	1.7×10^{-2}	41	64	7.4×10^{-4}	937	36

* Values of the first order rate constants, k, the half-time, $t_{1/2}$, and the percentage of the total microtubule population, %, were calculated based on Fig. 5 as described in the text.

control length after 3 min cold exposure (Fig. 9*c*). During the same time interval there was a 66% decrease in the number of microtubules per cell (Fig. 9*b*). Taking 112 s (Table II) as the half-time for polymer loss, the minimum rate of tubulin dissociation required to produce complete depolymerization of a 7.1-μm-long microtubule in 112 s was 103 dimers/s per microtubule. The actual rate of tubulin dissociation, once depolymerization is initiated, is likely to be much higher, since initiation of depolymerization appears to be the rate-limiting step. Based on the half-times for polymer loss (35 s for nocodazole treatment and 112 s for cold treatment), cooling to 3°C decreases the rate of initiation of depolymerization by 3.2-fold.

Disassembly of microtubules caused by nocodazole or cold temperature could be reversed by either washing out the drug or rewarming the cells to 37°C. Reassembly of microtubule polymer to near pre-treatment levels was observed within 20 min after rewarming of the cells or dilution of the drug (data not shown). Although the pattern of microtubule regrowth has not been analyzed in detail, the ability of the cells to regrow microtubules suggests that neither treatment caused irreversible damage to the cells.

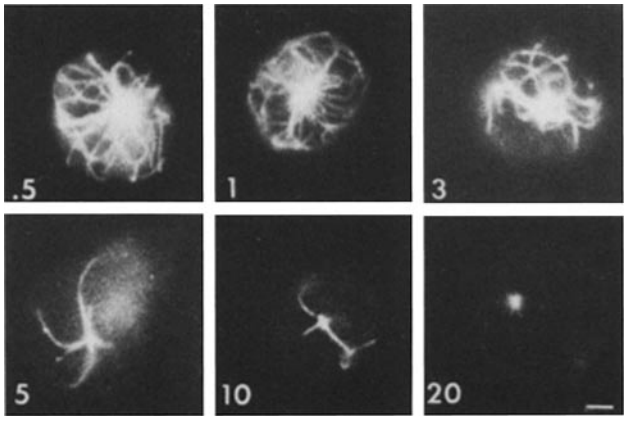

Figure 7. Immunofluorescent micrographs of the pattern of microtubule disassembly in monocytes after incubation at 3°C for the times (in minutes) indicated on each frame. Procedures were the same as described in the legend of Fig. 3. Control and 60-min incubation not shown. The pattern after 60 min is similiar to that found at 20 min. Cooling was complete within 8 s. Bar, 2 μm.

Discussion

Human monocytes have proved to be a useful cell type for quantitative analysis of microtubule behavior in vivo because the length of individual microtubules can be accurately measured using relatively simple immunofluorescence and video techniques. Overall, we have demonstrated that depolymerization of monocyte cytoplasmic microtubules, induced by nocodazole (10 μg/ml) or cold temperature (3°C), produced a rapid loss in total microtubule polymer (Figs. 5 and 9). This loss in microtubule polymer occurred by reduction in the number of microtubules and not by a simultaneous depolymerization of the entire microtubule population. Furthermore, the pattern of polymer loss is similiar with either nocodazole or cold temperature treatments, which suggests that the results are not artifacts of the particular depolymerizing agent.

Monocytes do not flatten completely on coverslips. The error in our length measurements in control cells is relatively small, on the order of 5% (see Materials and Methods). During microtubule depolymerization, cells usually round up. No attempts have been made to calculate cell height at each time point during depolymerization, but it seems reasonable to assume that there is a slightly larger error in length measurements at later time points during disassembly. This may contribute to the decrease in mean microtubule length seen during depolymerization.

With prolonged exposure to cold temperature, we see a small population of microtubules shorter than the original population (Figs. 9 and 10). Several possibilities exist to explain this observation. First, it is possible we had fixed microtubules in the process of depolymerization, and that this depolymerization was occurring from the distal ends inward. Second, there may have been some slow growth of a few microtubules under conditions where depolymerization was expected. This has been observed in vitro after dilution of the subunit pool well below the critical concentration for assembly (27, 28). Third, it is possible that some microtubule assembly occurred during the 15 s in lysis buffer before fixation, but there is no evidence to suggest this possibility.

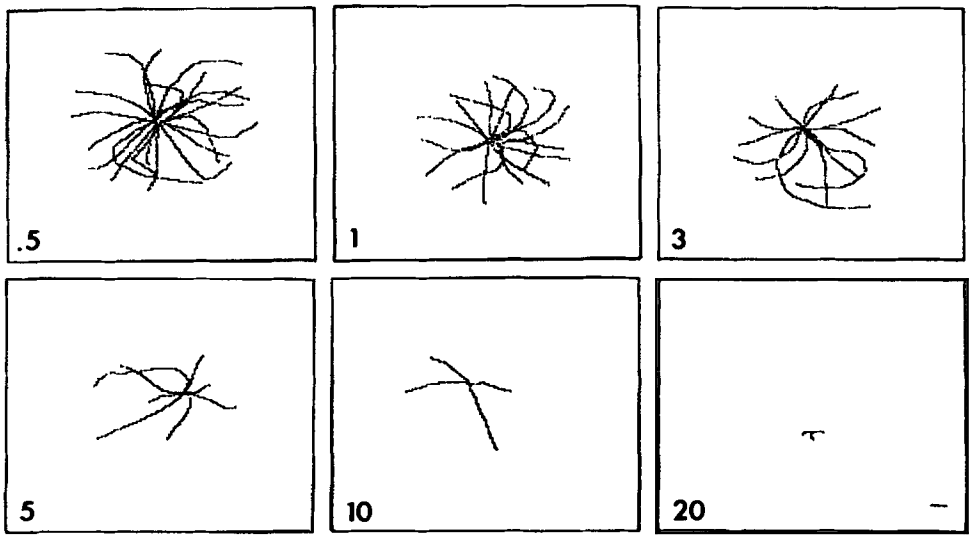

Figure 8. Examples of computer-generated line drawings of microtubule arrays obtained from single monocytes incubated at 3°C for the times indicated (in minutes) on each frame. These digitized images were obtained as described in the legend of Fig. 4, and were generated from different cells than those in Fig. 7. Bar, 1 μm.

Fourth, this observation may not represent normal microtubule behavior, since all cellular processes will be affected to some degree by exposure to cold temperature.

As shown in the length distribution histograms (Figs. 6 and 10), the rapid loss in microtubule polymer observed here was not consistent with a simultaneous shortening of all microtubules. A model based on synchronous depolymerization within two microtubule populations with very different rates of polymer loss was also not consistent with the experimental data (Figs. 6 and 10).

Alternately, the treadmilling model predicts that blockage of assembly would lead to a faster loss of tubulin subunits from the ends near the centrosome (−ends), with a slower loss of subunits from the distal (+) ends (23, 24). If this mechanism were occurring it should produce within a cell a number of shorter microtubules neither connected to the centrosome nor extending fully to the cell periphery. Our observations suggest that such a mechanism does not operate because we rarely saw short pieces of microtubules free in the cytoplasm. Recent evidence using FRAP of fluorescently la-

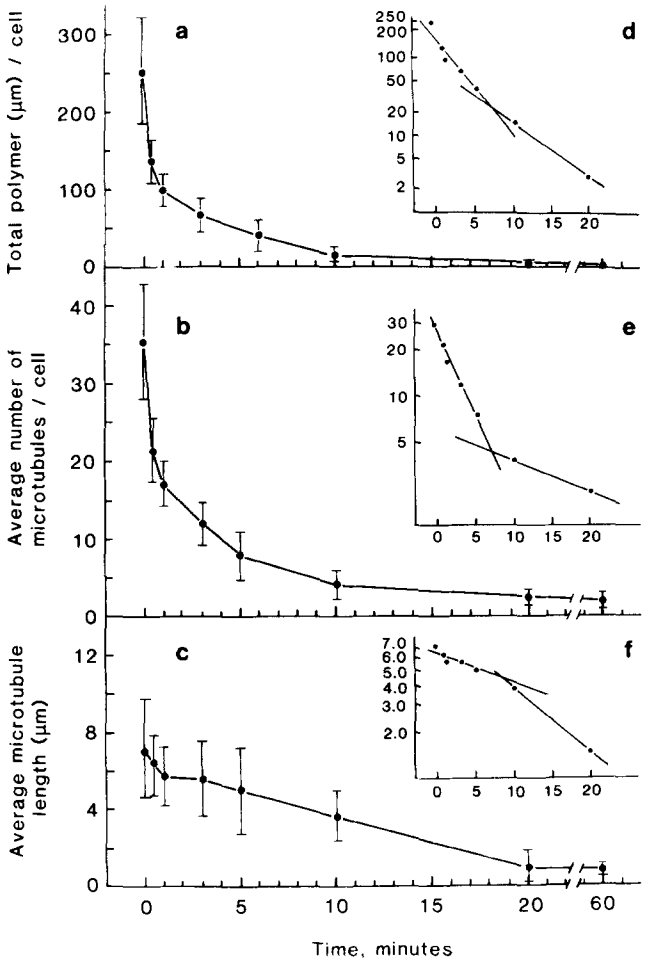

Figure 9. The changes in total polymer (*a*, linear scale; *d*, semilogarithmic scale), number of microtubules (*b*, linear scale; *e*, semilogarithmic scale), and average length (*c*, linear scale; *f*, semilogarithmic scale) per monocyte after depolymerization induced by incubation at 3°C. Each data point represents the average value of 10 cells, and the error bars correspond to the standard error of the mean.

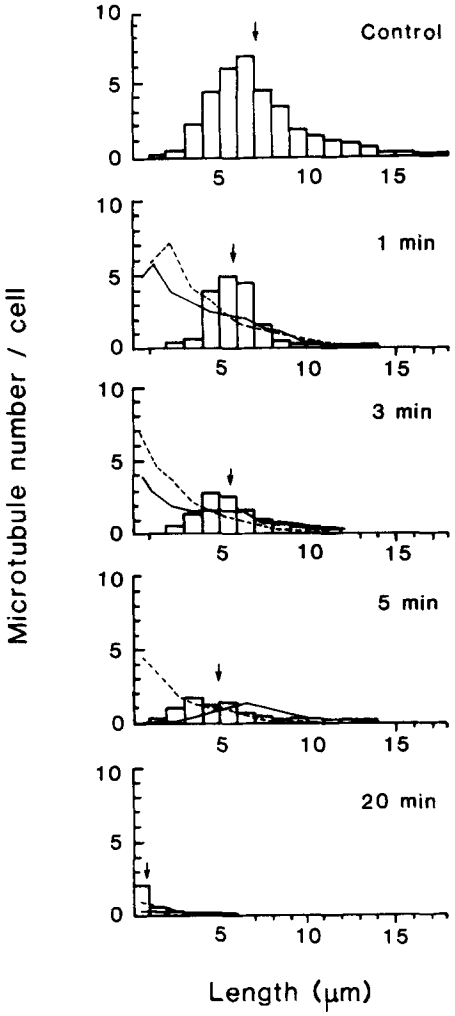

Figure 10. Histograms of the average distribution of microtubule lengths in monocytes after incubation at 3°C for the times given. Each histogram represents the average microtubule length distribution derived from 10 cells. Arrows denote mean length at each time point. Dashed lines represent theoretical length distributions for synchronous shortening of all microtubules at a constant rate as described in the legend of Fig. 6. The solid lines show theoretical depolymerization of two microtubule populations as described in the legend of Fig. 6.

*Table II. Biphasic Kinetics of Microtubule Depolymerization by Cold Temperature**

	Labile population			Differentially stable population		
	$k\ (s^{-1})$	$t_{1/2}\ (s)$	%	$k\ (s^{-1})$	$t_{1/2}\ (s)$	%
Loss in total polymer	6.2×10^{-3}	112	84	3.3×10^{-3}	210	16
Loss in microtubule number	5.0×10^{-3}	139	78	7.83×10^{-4}	885	22

* Values of the first order rate constants, k, the half-time, $t_{1/2}$, and the percentage of the total microtubule population, %, were calculated based on Fig. 9 as described in the text.

beled mitotic spindles and interphase microtubules in living cells also does not support the treadmilling hypothesis (31, 33, 34, 41, 42).

Theoretically, tubulin dissociation could also occur at sites distributed along the length of microtubules (13, 14), however, we have no direct evidence to support or refute this possibility. Once disassembly was initiated, the rate of depolymerization was too fast to allow determination of the site(s) of subunit dissociation by our experimental approach.

Our results are consistent with the persistent, individual behavior of microtubules as proposed by the Dynamic Instability model of Mitchison and Kirschner (28). When assembly was blocked in vivo, monocytes showed a dramatic decrease in microtubule number, with a slow change in mean microtubule length (Figs. 5 and 9). Preliminary results by McBeath and Fujiwara (26), with cultured cells from the inner surface of goldfish scales, also report an asynchronous pattern of microtubule depolymerization. Clearly, in monocytes, as well as BSCl, PtKl (6), and goldfish cells (26), the entire microtubule population does not respond in unison; there was a heterogeneous response, rather than a gradual shortening of all interphase microtubules. Consistent with Mitchison and Kirschner's prediction, it appeared that in monocytes the slow step in the process was the actual initiation of depolymerization. Once depolymerization began it was rapid and catastrophic.

There are several important consequences of our observation that the rate of initiation of depolymerization dominates the kinetics of disassembly of the entire microtubule population. Our minimum estimate of the rate of depolymerization of 329 dimers/s per microtubule for interphase microtubules is within the range estimated by Salmon et al. (32) for the depolymerization of sea urchin spindle microtubules after microinjection of colchicine. It seems possible then that spindle and interphase microtubules have similiar rates of depolymerization, with the increased lability of spindle microtubules due to a faster rate of initiation of disassembly. The asynchrony of microtubule disassembly in response to depolymerizing conditions may explain the uniform rate of decay of birefringence that occurs throughout the spindle after injection of colchicine (32, 42). Asynchronous microtubule turnover may also explain the rapid, uniform rate of tubulin incorporation throughout spindle fibers at steady-state assembly as shown recently by FRAP in both sea urchin embryos and mammalian cultured cells (31, 33, 41, 42). This asynchronous microtubule behavior at steady-state assembly also explains the slower, but uniform recovery of fluorescence after laser photobleaching of fluorescently labeled interphase microtubule arrays (33, 34).

Presently, the origins of the dynamic instability of the labile microtubules and the differential stability of a minor fraction of the microtubule population in the CMTC of monocytes is not understood. Because we have observed a catastrophic loss of entire microtubules in the labile population during disassembly, microtubules must be stabilized either by "capping" complexes at the microtubule ends (4, 5, 11, 17, 25, 27, 28, 43) or by the cooperative binding of stabilizing MAPs all along the length of a microtubule.

Mitchison and Kirschner have proposed, based in part on the work on Carlier and co-workers (4, 5, 11), that microtubules are stabilized by attachment of their proximal (−) end to the centrosome and by tubulin–GTP caps on their distal (+) ends. The microtubule core of tubulin–GDP is relatively unstable and when hydrolysis of tubulin–GTP catches up with the association of tubulin–GTP subunits at the microtubule ends, the microtubule will lose its cap and will depolymerize rapidly and completely. According to this model, the stability of microtubules growing from a centrosome is regulated solely by the distal cap of tubulin–GTP. In this regard, it would be useful to gain information on the site or sites of subunit loss during depolymerization in vivo. As stated previously, we have found that disassembly occurred at a rate too fast to allow conclusive determination of the site of subunit loss. McBeath and Fujiwara detected a loss of microtubules from the centrosome outward after cooling goldfish cells to −3°C (26). Whether or not this same phenomenon is true under more physiological conditions has not been determined.

GTP–tubulin caps may be responsible for the dynamic instability of the labile microtubule population, but additional mechanism(s) are required to produce the differential stability of some microtubules. Both DeBrabander et al. (7) and Bershadsky and Gelfand (2) demonstrated that cytoplasmic microtubules are stabilized against depolymerization when cells are treated with metabolic inhibitors. Inhibition of ATP production in vivo should result in a decreased GTP concentration, fewer tubulin–GTP caps, and thus the rapid depolymerization of microtubules. Therefore, tubulin–GTP caps cannot be the only microtubule stabilizing mechanism present in vivo.

Several other factors may be responsible for regulating microtubule stability. First, certain tubulin species may form more stable microtubules (9, 39). Although different tubulin subtypes have been identified, their functional significance in the CMTC has not been established. Second, MAPs may bind to a limited subset of microtubules and result in increased microtubule stability. Third, as suggested by the data with metabolic inhibitors, modification of MAPs may lead to microtubule stability. This could result from tight binding of dephosphorylated MAPs (15, 18). In this regard it is interesting to note the much slower loss of microtubule polymer we see in cold-treated cells. This difference in rate could be the consequence of reduced ATP levels at lower temperatures.

In summary, monocyte microtubules depolymerize rapidly once depolymerization is initiated, but initiation is asynchronous throughout the microtubule population when assembly is abruptly blocked. The labile microtubules comprise 70–84% of the total microtubule population, the remaining 16–30% of the population is differentially stable. The rate limiting step for disassembly appears to be the initiation of depolymerization. The data presented here are predicted by the Dynamic Instability model (28) of microtubule assembly, but the origin of microtubule instability and differential stability remains unknown.

We are grateful to Winthrop Jackman for generously allowing repeated puncture of his fingers for blood cells. Thanks also to the lab of Dr. M. Cohen, University of North Carolina, for providing us with cells. Thanks to N. Pryer, T. Hays, M. Caplow, and K. Przywansky for many helpful discussions and Nancy Salmon for editorial assistance. The monoclonal antibody to tubulin was from the lab of J. R. McIntosh. We also thank David Newton for help with computer programming, and Nancy Lucas for performing statistical analysis.

Received for publication 25 November 1985, and in revised form 10 January 1986.

References

1. Anderson, D. C., L. J. Wible, B. J. Hughes, C. W. Smith, and B. R. Brinkley. 1982. Cytoplasmic microtubules in polymorphonuclear leukocytes: effect of chemotactic stimulation and colchicine. *Cell.* 31:719–729.
2. Bershadsky, A. D., and V. I. Gelfand. 1983. Role of ATP in the regulation of stability of cytoskeletal structures. *Cell Biol. Int. Rep.* 7:173–187.
3. Brinkley, B. R., S. H. Fistel, J. M. Marcum, and R. L. Pardue. 1980. Microtubules in cultured cells; indirect immunofluorescent staining with tubulin antibody. *Int. Rev. Cytol.* 63:59–95.
4. Carlier, M., and D. Pantaloni. 1981. Kinetic analysis of guanosine 5′-triphosphate hydrolysis associated with tubulin polymerization. *Biochemistry.* 20:1918–1924.
5. Carlier, M., T. L. Hill, and Y. Chen. 1984. Interference of GTP hydrolysis in the mechanism of microtubule assembly: an experimental study. *Proc. Natl. Acad. Sci. USA.* 81:771–775.
6. Cassimeris, L., M. Tioran, P. Wadsworth, and E. D. Salmon. 1985. Dynamic instability of cytoplasmic microtubules in vivo. *J. Cell Biol.* 101 (5, Pt. 2):24a. (Abstr.)
7. DeBrabander, M., G. Geuens, R. Nuydens, R. Willebrords, and J. DeMey. 1980. The microtubule nucleating and organizing activity of kinetochores and centrosomes in living PtK2 cells. *In* Microtubule and Microtubule Inhibitors. M. DeBrabander and J. DeMey, editors. Elsevier/North-Holland Biomedical Press, Amsterdam. 57–70.
8. Deery, W. J., A. R. Means, and B. R. Brinkley. 1984. Calmodulin-microtubule association in cultured mammalian cells. *J. Cell Biol.* 98:904–910.
9. Gunderson, G. G., M. H. Kalnoski, and J. C. Bulinski. 1984. Distinct populations of microtubules: tyrosinated and nontyrosinated alpha tubulin are distributed differently in vivo. *Cell.* 38:779–789.
10. Hill, T. L., and M. W. Kirschner. 1982. Bioenergetics and kinetics of microtubule and actin filament assembly-disassembly. *Int. Rev. Cytol.* 78:1–125.
11. Hill, T. L., and M. Carlier. 1983. Steady-state theory of the interference of GTP hydrolysis in the mechanism of microtubule assembly. *Proc. Natl. Acad. Sci. USA.* 80:7234–7238.
12. Hoebeke, J., G. Van Nijen, and M. DeBrabander. 1976. Interaction of oncodazole (R17934), a new antitumoral drug, with rat brain tubulin. *Biochem. Biophys. Res. Commun.* 69:319–324.
13. Inoue, S., and H. Ritter. 1975. Dynamics of mitotic spindle organization and function. *In* Molecules and Cell Movements. S. Inoue and R. E. Stephens, editors. Raven Press, New York. 3–29.
14. Inoue, S. 1981. Cell division and the mitotic spindle. *J. Cell Biol.* 91 (3,Pt.2):131s–147s.
15. Jameson, L., and M. Caplow. 1981. Modification of microtubule steady-state dynamics by phosphorylation of the microtubule-associated proteins. *Proc. Natl. Acad. Sci. USA.* 78:3413–3417.
16. Johnson, K. A., and G. G. Borisy. 1977. Kinetic analysis of microtubule self-assembly in vitro. *J. Mol. Biol.* 117:1–31.
17. Job, D., C. T. Rauch, E. H. Fischer, and R. L. Margolis. 1982. Recycling of cold-stable microtubules: evidence that cold stability is due to substoichiometric polymer blocks. *Biochemistry.* 21:509–515.
18. Job, D., M. Pabion, and R. L. Margolis. 1985. Generation of microtubule stability subclasses by microtubule-associated proteins: implications for the "Dynamic Instability" model. *J. Cell Biol.* 101:1680–1689.
19. Karsenti, E., S. Kobeyashi, T. Mitchison, and M. Kirschner. 1984. Role of centrosomes in organizing the interphase microtubule array: properties of cytoplasts containing or lacking centrosomes. *J. Cell Biol.* 98:1763–1776.
20. Keith, C. H., J. R. Feramisco, and M. Shelanski. 1981. Direct visualization of fluorescein-labeled microtubules in vitro and in microinjected fibroblasts. *J. Cell Biol.* 88:234–240.
21. Lee, C., D. J. Field, and L. L. Y. Lee. 1980. Effects of nocodazole on structures of calf brain tubulin. *Biochemistry.* 19:6209–6215.
22. Lewis, A. E. 1984. Biostatistics. Van Nostrand Reinhold Company, New York.
23. Margolis, R. L., and L. Wilson. 1978. Opposite end assembly and disassembly of microtubules at steady state in vitro. *Cell.* 13:1–8.
24. Margolis, R. L., and L. Wilson. 1981. Microtubule treadmills-possible molecular machinery. *Nature (Lond.).* 293:705–711.
25. Margolis, R. L., and C. T. Rauch. 1981. Characterization of rat brain crude extract microtubule assembly: correlation of cold stability with the phosphorylation state of a microtubule-associated 64K protein. *Biochemistry.* 20:4451–4458.
26. McBeath, E., and K. Fujiwara. 1985. Kinetics of temperature induced microtubule assembly and disassembly in cells studied by immunofluorescence. *J. Cell Biol.* (5, Pt. 2):25a. (Abstr.)
27. Mitchison, T., and M. Kirschner. 1984. Microtubule assembly nucleated by isolated centrosomes. *Nature (Lond.).* 312:232–237.
28. Mitchison, T., and M. Kirschner. 1984. Dynamic instability of microtubule growth. *Nature (Lond.).* 312:237–242.
29. Osborn, M., and K. Weber. 1976. Cytoplasmic microtubules in tissue culture cells appear to grow from an organizing structure towards the plasma membrane. *Proc. Natl. Acad. Sci. USA.* 3:867–871.
30. Pickett-Heaps, J. D. 1969. The evolution of the mitotic apparatus: an attempt at comparative ultrastructural cytology in dividing plant cells. *Cytobios.* 3:257–280.
31. Salmon, E. D., R. J. Leslie, W. M. Saxton, M. L. Karow, and J. R. McIntosh. 1984. Spindle microtubule dynamics in sea urchin embryos: analysis using a fluorescein-labelled tubulin and measurements of fluorescence redistribution after laser photobleaching. *J. Cell Biol.* 99:2165–2174.
32. Salmon, E. D., M. McKeel, and T. Hays. 1984. Rapid rate of tubulin dissociation from microtubules in the mitotic spindle in vivo measured by blocking polymerization with colchicine. *J. Cell Biol.* 99:1066–1075.
33. Saxton, W. M., D. L. Stemple, R. J. Leslie, E. D. Salmon, M. Zavortink, and J. R. McIntosh. 1984. Tubulin dynamics in cultured mammalian cells. *J. Cell Biol.* 99:2175–2186.
34. Scherson, T., T. E. Kries, J. Schlessinger, U. Z. Littauer, G. G. Borisy, and B. Geiger. 1984. Dynamic interactions of fluorescently labeled microtubule-associated proteins in living cells. *J. Cell Biol.* 99:425–434.
35. Schliwa, M. 1980. Pharmacological evidence for an involvement of calmodulin in calcium-induced microtubule disassembly in lysed tissue culture cells. *In* Microtubules and Microtubule Inhibitors. M. DeBrabander and J. DeMey, editors. Elsevier/North-Holland Biomedical Press, Amsterdam. 57–70.
36. Schliwa, M., K. B. Pryzwansky, and U. Euteneuer. 1982. Centrosome splitting in neutrophils: an unusual phenomenon related to cell activation and motility. *Cell.* 31:705–717.
37. Scholey, J. M., B. Neighbors, J. R. McIntosh, and E. D. Salmon. 1984. Isolation of microtubules and a dynein-like MgATPase from unfertilized sea urchin eggs. *J. Biol. Chem.* 259:6516–6525.
38. Soltys, B. J., and G. G. Borisy. 1985. Polymerization of tubulin in vivo: direct evidence for assembly onto microtubule ends and from centrosomes. *J. Cell Biol.* 100:1682–1689.
39. Thompson, W. C., D. J. Asai, and D. H. Carney. 1984. Heterogeneity among microtubules of the cytoplasmic microtubule complex detected by a monoclonal antibody to alpha tubulin. *J. Cell Biol.* 98:1017–1025.
40. Wadsworth, P., and R. D. Sloboda. 1983. Microinjection of fluorescent tubulin into dividing sea urchin eggs. *J. Cell Biol.* 97:1249–1254.
41. Wadsworth, P., and E. D. Salmon. 1986. Analysis of the treadmilling model during metaphase of mitosis using fluorescence redistribution after photobleaching. *J. Cell Biol.* 102:1032–1038.
42. Wadsworth, P., and E. D. Salmon. 1986. Microtubule dynamics in mitotic spindles of living cells. *Ann. NY Acad. Sci.* In press.
43. Webb, B. C., and L. Wilson. 1980. Cold-stable microtubules from brain. *Biochemistry.* 19:1992–2001.